Vibrational Study of the FeCl 3 −Doped Dimer of Polyaniline; A Good Model Compound of Emeraldine Salt

ARTICLE *in* THE JOURNAL OF PHYSICAL CHEMISTRY B · SEPTEMBER 2000

Impact Factor: 3.3 · DOI: 10.1021/jp000946v

Vibrational Study of the $FeCl_3$-Doped Dimer of Polyaniline; A Good Model Compound of Emeraldine Salt

M. I. Boyer, S. Quillard,* G. Louarn, G. Froyer, and S. Lefrant

Laboratoire de Physique Cristalline, Institut des Matériaux Jean Rouxel, Boite Postale 32229, 44322 Nantes Cédex 03, France

Received: March 13, 2000; In Final Form: May 24, 2000

In this paper, optical and vibrational properties of the $FeCl_3$-doped dimer of polyaniline, a model compound of emeraldine salt are presented. This oligomer is synthesized according to the method reported by Zaghal et al.. A complete assignment of the fundamental in-plane Raman and infrared modes (1700−600 cm^{-1}) of this oligoaniline is proposed. The observed frequencies of the dark blue microcrystals are compared with those acquired by vibrational calculations based on a valence force field model. To show, by a most efficient way, the evolution of the electronic configuration of the dimer upon doping, the experimental vibrational modes of the doped dimer and its related force constants are compared with those of its fully reduced and oxidized forms. The strongly aromatic and semiquinone-like characters of the rings present in the doped dimer is put in evidence by Resonance Raman Scattering and infrared absorption and confirmed by vibrational calculations. Considering the numerous similarities between the vibrational characteristics of the polymeric chain and its well-defined oligomer, this study also provides useful information about the electronic configuration of the protonated emeraldine, which remains under debate.

1. Introduction

Conjugated polymers have attracted considerable attention since the discovery of possible insulator-to-"metal" transitions in these systems. In the electroactive polymers field, polyaniline has been one of the most studied substances during the past 10 years, in particular because of its interesting electrooptical properties. The polyaniline family, whose general formula of the base forms is schematically depicted in Figure 1, refers to a complex polymer class exhibiting several possible structures according to the value of the average oxidation state $1 - y$. The variable y corresponds to the ratio within the repeat unit of the number of nitrogen atoms of amine type over the total number of nitrogen atoms. Depending on the y value, the three insulating base forms of polyaniline, the colorless (or pale yellow) leucoemeraldine ($y = 1$), the blue emeraldine ($y \approx 0.5$), and the purple pernigraniline ($y = 0$) are discerned.[1−3] The polyaniline family is also characterized by its degree of protonation. Thus, the acidic protonation of emeraldine base[4] or the oxidation of leucoemeraldine base in a sufficient acidic medium gives the green emeraldine salt (ES), the only conducting form of polyanilines (Figure 2).

Although the polyaniline family attracts a considerable interest,[5] due in particular to its good environmental stability[6] and its low cost, the electronic configuration of the conducting form, ES, is still the subject of controversy, which constitutes a limiting factor for potential applications such as rechargeable battery electrodes,[7] smart windows,[8] various types of sensors,[9−12] anticorrosion coating, and so forth.[13,14] According to different authors, the opinions diverge between the polaronic lattice and the bipolaronic form[15] (see again Figure 2).

Regarding the large literature devoted to conjugated conducting polymers such as polyacetylene, poly(*p*-phenylene), polypyrrole, and polythiophene, a model compounds approach has clearly been proven to be a suitable method to acquire information about an intractable polymeric chain from the electrochemical, optical, electronic, and magnetic viewpoints.[16−20] In particular, a detailed vibrational study (Raman Scattering and infrared (IR) absorption spectroscopies combined with dynamical calculations or quantum chemical calculations) of oligomers with precisely defined length and constitution has shown to provide information not only about the molecular vibrations of the compounds under study and the corresponding polymeric chain but also about their electronic configuration.[21−24] Indeed, Raman and IR spectroscopies are highly sensitive to even small structural or electronic alterations.[25] This is particularly true in the field of the conducting polymers, where, due to the strong electron−lattice coupling, the dopant−polymer charge transfer results in the creation of defects such as solitons, polarons, and bipolarons.[26−29] Moreover, a particular case of Raman Scattering, called Resonant Raman Scattering (RRS) spectroscopy, is of a particular interest upon the evaluation of the doping induced changes. This Resonance Raman effect occurs when the scattering system has an absorption band close to the excitation frequency and induces an enhancement of the Raman lines associated to the chromophore. Conducting polymers and their oligomers, which usually show electronic absorptions due to self-localized excitations in the region from visible to near-infrared, are subject to RRS effect. Thus, by selecting an adequate excitation wavelength, the features of the polaronic lattice and the bipolaronic defects can be resonantly enhanced.

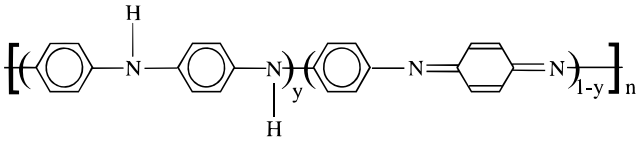

Figure 1. Schematic structure of the base forms of polyaniline family.

* Corresponding author. sophie.quillard@cnrs-imn.fr

10.1021/jp000946v CCC: $19.00
Published on Web 09/01/2000

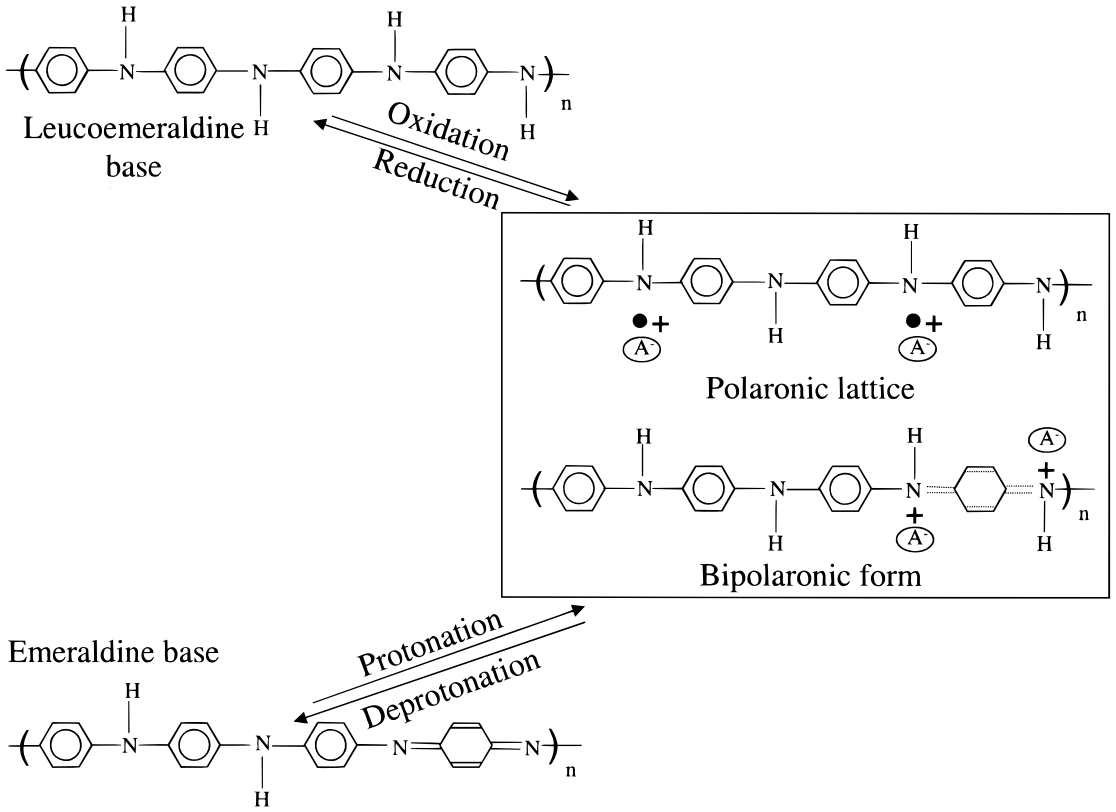

Figure 2. Schematic representation of the polaronic lattice and the bipolaronic form of emeraldine salt.

These charged defects can be selectively put in evidence via the vibrational study of radical cation (polaron) and dication (bipolaron) of convenient model compounds.

The purpose of this work consists of obtaining information about the vibrational properties and the electronic structure of ES by using a model compounds approach combined with a vibrational study. The model molecule of ES, the chlorine salt form of the dimer, is obtained by chemical oxidation of N,N′ diphenyl-1,4-phenylenediamine with $FeCl_3$ according to the Zaghal et al. procedure.[30] Its study is conducted to furnish information about the vibrational properties and the electronic configuration of the polaronic lattice of ES. In a first part, the synthesis route and the optical properties of the $FeCl_3$-doped dimer are presented. In a second part, the assignment of the fundamental modes, ranged in the 1700−600 cm^{-1} domain, is proposed. A selective enhancement of the vibrational bands relative to the two kinds of units present in this molecule is achieved upon excitation in resonance with the 387 and 700 nm transitions. In this study, a comparison with the vibrational characteristics of the reduced phenyl end-capped dimer referred to as B3 (N,N′ diphenyl-1,4-phenylenediamine) and its oxidized form, referred to as B2Q1 (N,N′ diphenyl-1,4-benzoquinone-diimine), is presented (Figure 3).[31,2] And finally, to confirm the proposed assignment, the vibrational calculations were performed.

2. Experimental Section

A. **Synthesis.** The reduced dimer (B3) was purchased from Aldrich and recrystallized three times from toluene. The $FeCl_3$-doped dimer was prepared in good yield by chemical oxidation of B3 with iron hexahydrate trichloride ($FeCl_3$-$6H_2O$), according to the procedure of Zaghal and Shatnawi.[30] This doped dimer comes in the form of dark blue microscopic crystals. X-ray dispersion energy experiment shows that upon electron acceptor

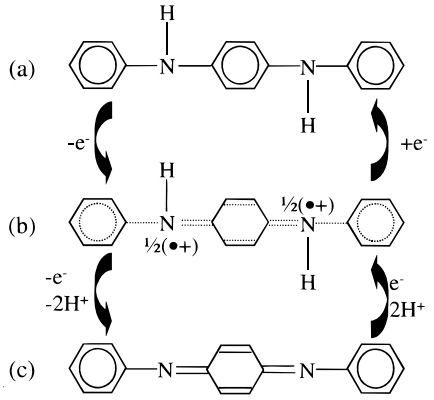

Figure 3. Schematic representation of (a) N,N′ diphenyl-1,4-phenylenediamine (B3), (b) the $FeCl_3$ doped dimer, and (c) N,N′ diphenyl-1,4-benzoquinonediimime (B2Q1).

doping (p-type doping), a paramagnetic (Electron Paramagnetic Resonance measurements) radical cation salt consisting of a positively charged dimer and a Cl^- counterion is formed. The completely oxidized form of the dimer (B2Q1) was synthesized also according to the Zaghal et al. procedure.

B. **Spectroscopic Investigations.** UV−vis absorption spectra of the dimer in its various oxidation states are recorded on a Varian Cary 5G at room temperature (RT). UV−vis characteristics are obtained in acetonitrile medium (+ diphenyl phosphate for the $FeCl_3$-doped dimer).

Infrared absorption spectra are collected with a Nicolet 20 SXC FTIR spectrometer equipped with a DTGS detector. The data are registered by transmission (KBr pellets technique) at RT. A 2 cm^{-1} spectral resolution is taken for the experiments and the spectra are corrected from the KBr signal.

The Raman Scattering spectra are measured with several laser lines ranging from 457.9 to 1064 nm. Raman characteristics obtained with the excitation lines in the visible range (457.9,

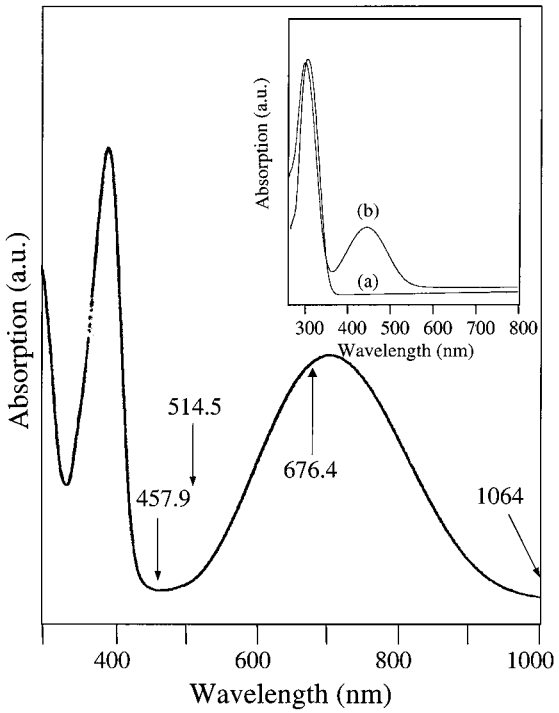

Figure 4. UV−vis absorption spectra of the doped dimer in acetonitile plus diphenyl phosphate solution (the UV−vis data of (a) B3 and (b) B2Q1 in acetonitrile medium in the insert are shown).

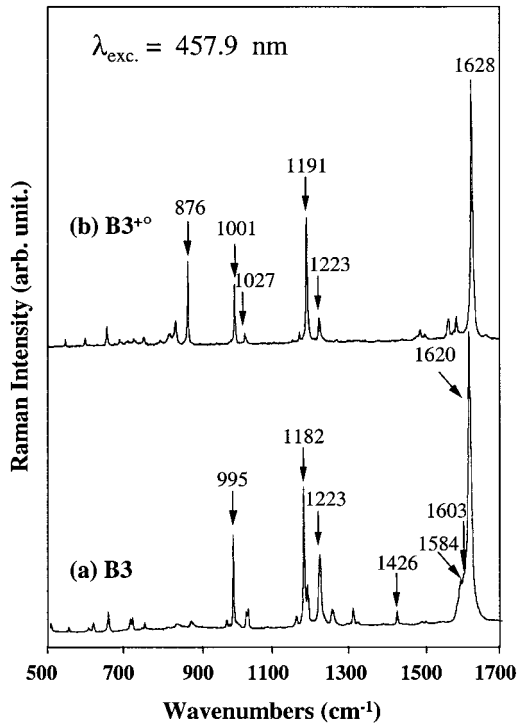

Figure 5. Raman spectra of (a) B3 and (b) the doped dimer at an excitation wavelength of 457.9 nm.

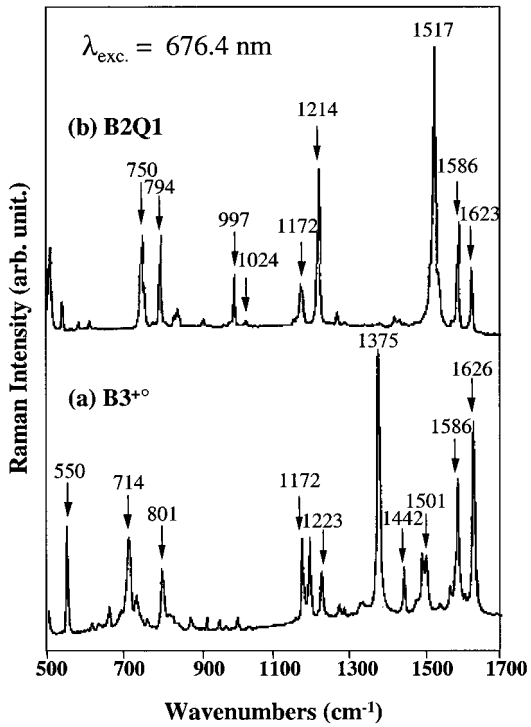

Figure 6. Raman spectra of (a) the doped dimer and (b) B2Q1 at an excitation wavelength of 676.4 nm.

514.5 nm with an argon ion laser and 676.4 nm with an Krypton ion laser) are recorded using a multichannel Jobin−Yvon T64000 spectrometer connected to a liquid nitrogen cooled charged-coupled device detector (resolution ∼2 cm^{-1}). The scattering signal is collected with a backscattering geometry under microscope. To avoid any problem of degradation that occurs at RT, the data are registered at liquid nitrogen temperature (77 K) and at a power beam of ca. 1 mW. Raman spectra excited at the near-infrared laser radiation (1064 nm Nd: YAG laser) are measured on a FT-Raman spectrophotometer (RFS 100 Bruker) at RT.

3. Results and Discussion

A. **UV−Vis Absorption Spectroscopy.** The optical absorption spectrum of the doped dimer is reported in Figure 4 (acetonitrile absorption is substrated). In the insert of Figure 4, we show those of B3 and B2Q1. In acetonitrile, B3 absorbs at 302 nm (4.11 eV), whereas B2Q1 is characterized by an additional absorption band centered at 442 nm (2.81 eV). Upon doping of the reduced dimer with iron trichloride, the oligomer shows strong absorptions in the visible range, which makes it suitable for Resonance Raman studies. Indeed, two absorption bands emerge around 387 (3.18 eV) and 700 nm (1.77 eV). These absorptions are characteristic of the radical cation of the dimer. They are also present in the absorption spectra of its homologous obtained by an electrochemical way in an acetonitrile + diphenyl phosphate electrolyte.[32]

B. **Raman and Infrared Spectroscopies.** In this part, we describe the fundamental in-plane vibrational modes of the $FeCl_3$-doped dimer in the spectral range 1700−600 cm^{-1}. The assignment of the bands in the 3600−2700 cm^{-1} frequency range is not discussed because experimental frequencies are more numerous than those predicted by group theory (combination and overtones). However, the peaks in the 3100−3000 cm^{-1} spectral domain are ascribed without ambiguity to the C−H stretching modes.

The Raman spectra of the $FeCl_3$-doped molecule performed at 457.9 and 676.4 nm are presented in Figures 5 and 6, respectively. At these wavelengths, we are observing preresonance and resonance conditions with the 387 and 700 nm absorption bands, respectively. Only the data obtained at 676.4 nm are discussed because the spectral patterns taken with the 514.5, 676.4, and 1064 nm lines (Figure 7) are practically comparable. Indeed, whatever the excitation lines used (514.5 → 1064 nm), no frequency dispersion is observed, but only the

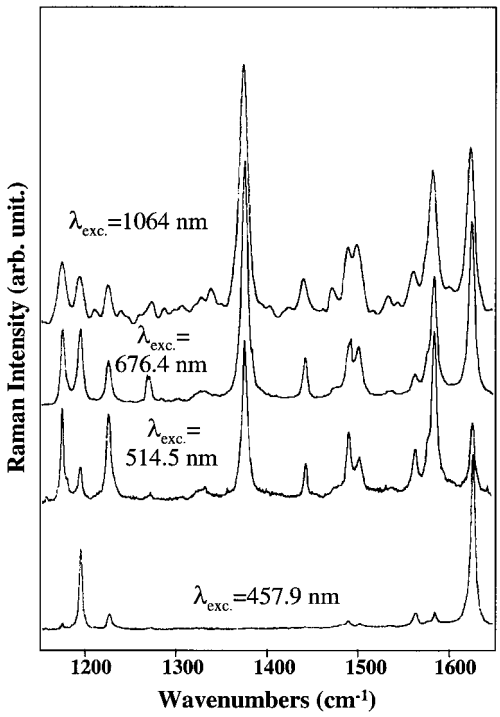

Figure 7. Raman spectra of the doped dimer at various excitation wavelengths.

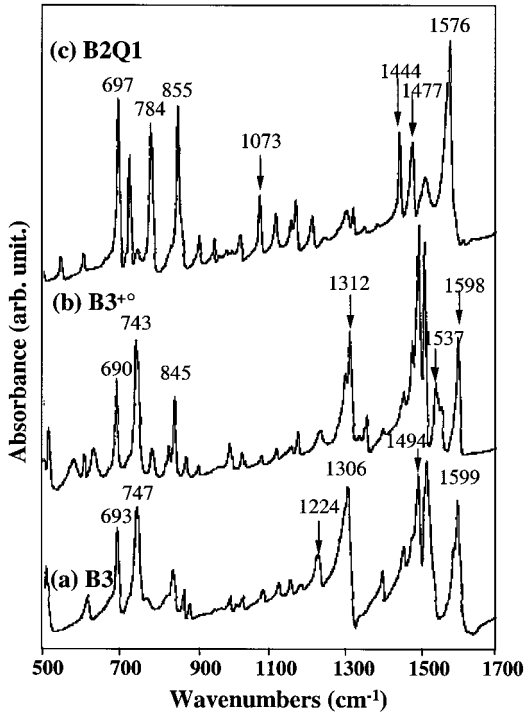

Figure 8. Infrared spectra of (a) B3, (b) the doped dimer, and (c) B2Q1.

relative intensities vary from one wavelength to the other. To more easily follow the evolution of the characteristic bands upon the degree of oxidation, the vibrational fingerprints of the doped molecule are compared to those of B3 (at 457.9 nm) and B2Q1 (at 676.4 nm). An analogy with the vibrational features of emeraldine salt will also be given.[33,34]

Infrared spectra of the dimer in its three distinct oxidation states are shown in Figure 8. Because of the large number of experimental absorptions, mainly, the vibrational characteristics of the inner ring of the doped dimer will be examined. Indeed, as we will show in the following parts, the IR bands of the outer rings are rather slightly sensitive to the central ring nature, and the monosubstituted groups possess an aromatic-like character.

For simplicity, in the subsequent text, the most characteristic spectral ranges will be discussed separately and the well-known Wilson's notation,[35] established for the benzene ring vibrations, will be adopted for the ring modes. The experimental frequencies are collected in Tables 1 and 2.

(a) Region I: 1700−1400 cm^{-1}. The 1700−1400 cm^{-1} spectral range is of a particular interest because it corresponds to the domain of the ring CC stretching modes. Its study consequently furnishes information about the aromatic, semiquinone, or quinoid-like character of the rings present in the molecule or macromolecule under investigation. The study of this range is also important because the Raman spectrum of the doped dimer performed at 457.9 nm is quasi similar to the one of the corresponding polymeric form at the same excitation wavelength.[36] As shown in Figure 7, the Raman characteristics of the three rings model molecule of ES differ only slightly according to the excitation wavelengths except at 457.9 nm. Thus, the spectrum performed at 676.4 nm is particularly rich in bands, whereas the one obtained at 457.9 nm contains a single intense band peaked at 1628 cm^{-1}. Using the blue excitation line, this peak is followed at low frequency by a series of bands observed at 1586, 1564, 1501, and 1490 cm^{-1}. These bands, of low intensity at this wavelength, are strongly enhanced with the red line. The IR spectrum of the $FeCl_3$-doped dimer exhibits numerous absorptions that are due in majority to the two outer monosubstituted rings vibrations.

The Raman line at high frequency (1628 cm^{-1}), intense and sharp for all the excitation wavelengths available, is assigned to the C−C stretching vibrations (8a mode according to the Wilson nomenclature) of the two monosubstituted rings. The equivalent mode appears at 1603 and 1623 cm^{-1} in the spectra of B3 and B2Q1. The 8a mode (paradisubstituted ring) gives rise to a broad band pointed at 1626 cm^{-1} in the spectrum of ES. Let us note that the sharpness of the bands relative to the doped dimer with regard to those of the polymeric chain probably accounts for a stronger localization of the charge in the three rings model molecule. In the infinite chain, the bandwidth increase can be associated to a more extended delocalization of the charge (more than one unit) or/and to the mixture of several bands close in frequency. The 8a mode of the outer groups is also distinguishable at 1598 cm^{-1} in the IR spectrum of the doped dimer. This ring mode is observed at the same frequency for B3. The homologous of the 8a mode, the C−C stretching 8b mode, is rather difficult to discern because this mode is known to give rise to a band of low intensity in this family. However, the very weak band at 1603 cm^{-1} is ascribed to this ring mode.

For the inner ring, the stretching 8a mode of its C≈C bonds non adjacent to the N−H group occurs at 1586 cm^{-1}. The equivalent mode is peaked at 1581 cm^{-1} in the spectrum (676.4 nm) of the polymer. This ring mode vibrates at the same frequency in the B2Q1 case. However, the inner group of the dimer does not possess a quinoid character. Indeed, the band present at 1415 cm^{-1} in the spectrum of B2Q1, described as the stretching 8b vibrational mode of the C−C bonds adjacent to the imine group, is not observable in the Raman spectra of the radical cation. The peak at 1490 cm^{-1} intense with the red line, arises probably from the C∼C stretching 8b mode of the central ring of the radical because its intensity evolution is similar to this of the 8a mode at 1586 cm^{-1} passing from 514.5

TABLE 1: Experimental and Calculated Raman Frequencies of the $FeCl_3$-Doped Dimer, Experimental Raman Frequencies of Emeraldine Salt, Potential Energy Distribution (values less than 10% are neglected) on the $FeCl_3$-Doped Dimer, and Proposal of Assignment.

Wilson notation	$FeCl_3$-doped dimer exp	$FeCl_3$-doped dimer calc	emeraldine salt (exp.)[33]	PED (%) obtained on the $FeCl_3$-doped dimer	proposal of assignment
8a (B)	1628	1628	1626	$51K_t + 27H_\phi + 20K_{t'}$	C−C stretch (B)
8b (B)	1603	1612		$38K_t + 35K_{t'} + 21H_\phi$	C−C stretch (B)
8a (SQ)	1586	1584	1581	$69K_{SQD} + 16H_{SQ\phi} + 15K_{SQt}$	C≈C stretch (SQ)
19a (B)	/[a]	1521		$57H_\phi + 22K_t + 14K_{t'}$	C−C stretch + C−H def (B)
N−H	1501	1503	1512	$32H_{\delta'} + 25H_\delta + 14H_\phi$	sym N−H def.
8b (SQ)	1490	1478	1484	$36H_\phi + 19K_{SQt} + 19K_t$	C∼C stretch (SQ)
19b (B)	/	1478		$33H_\phi + 15K_t + 23F_{Qt}$	C−H def + C−C stretch (B)
C∼N + 3 (SQ)	1375	1409		$26K_{SQR'} + 22H_{SQ1\phi} + 18K_{SQt}$	C∼N stretch + C−H def (B)
C∼N	1375	1375	1311/1332	$56K_{SQR'} + 11H_{SQ1\phi}$	sym C∼N stretch
3 (B)	1327	1359		$91H_\phi$	C−H def (B)
3 (SQ)	1282	1315		$39H_\phi + 23K_{t'} + 19K_t + 13F_{Q\phi} + 11F_{Q1\phi}$	C−H def (SQ)
14 (B)	1270	1252	1253	$32H_\phi + 21K_{t'} + 17K_{SQt}$	ring def (B)
C−N	1223	1225		$41K_{SQR} + 25H_\phi$	C−N stretch
9a (B)	1191	1193	1192	$64H_\phi + 19K_t$	C−H def (B)
9a (SQ)	1172	1170	1166	$44H_{SQ1\phi} + 31H_{SQ\phi} + 13K_{SQD}$	C−H def (SQ)
15 (B)	1154	1158		$81K_t + 26K_{t'} - 27F^o_{(t,t)}$	ring def (B)
18b (B)	/	1089		$42K_t + 42H_\phi$	C−H def (B)
18a (B)	1027	1033		$32H_\phi + 30K_t + 16H_\alpha$	C−H def (B)
1+12 (B)	1001	988		$39K_t + 24H_\alpha + 13K_{t'}$	ring def (B)
1 (B)			886		ring def (B)
6a (B)	828	832		$29H_\alpha + 20K_{t'} + 16K_{SQR}$	X-sensitive (B)
1 (SQ)	801	805	810	$64K_{SQt}$	ring def (SQ)
6a (SQ)	659	667		$20H_{SQ\alpha} + 19H_{SQ\delta'} + 15H_\alpha$	X-sensitive (SQ)
6b (B)	602	607	608	$62H_\alpha + 15H_\phi$	ring def (B)
6b (SQ)	614	604		$40H_{SQ\alpha} + 23K_{SQt}$	ring def (SQ)

[a] / means not observable

TABLE 2: Experimental and Calculated Infrared Frequencies of the $FeCl_3$-Doped Dimer, Experimental Infrared Frequencies of Emeraldine Salt, Potential Energy Distribution (values less than 10% are neglected) on the $FeCl_3$-Doped Dimer, and Proposal of Assignment

Wilson notation	$FeCl_3$-doped dimer exp	$FeCl_3$-doped dimer calc	emeraldine salt (exp)[34]	PED (%) obtained on the $FeCl_3$-doped dimer	proposal of assignment
8a(B)	1598	1628	1608	$50K_t + 27H_\phi + 20K_{t'}$	C−C stretch (B)
8b(B)	1591	1612		$39K_t + 35K_{t'} + 22H_\phi$	C−C stretch (B)
19b(SQ)	1553	1563	1558	$78K_{SQD} + 13H_{SQ\phi} + 13K_{SQt}$	C≈C stretch + C−H def (SQ)
19a(B)	1509	1520		$58H_\phi + 22K_t + 14K_{t'}$	C−C stretch + C−H def (B)
N−H	1537	1499	1477	$22H_\phi + 28H_{\delta'} + 25H_\delta$	asym N−H def
19b(B)	1453	1462		$18H_\phi + 16H_{\delta'} + 15K_{SQt} + 10K_t$	C−C stretch + C−H def (B)
19a(SQ)+**C**∼N	1447	1450		$33K_{SQR'} + 16H_{SQ1\phi} + 17K_{SQt}$	C∼N stretch + C−H def (SQ)
19a(SQ)+C∼N	1355	1343	1356	$27H_\phi + 28K_{SQR'} + 22H_{SQ1\phi}$	C∼N stretch + C−H def (SQ)
3(B)	1337	1366		$69H_\phi + 29K_{SQR'} + 18H_{SQ1\phi}$	C−H def (B)
14(B)	1312	1322		$36H_\phi + 29K_t + 20K_{Qt}$	C−H def (B)
14(SQ)	1232	1257	1246	$31H_\phi + 21K_{t'} + 20K_{Qt}$	C−H def (SQ)
C−N	/[a]	1226		$40K_{SQR} + 27H_\phi$	asym C−N stretch
9a(B)	1174	1193	1178	$65H_\phi + 19K_t$	C−H def (B)
15(B)	1156	1161		$73K_t - 23F^o_{(t,t)} + 23K_{t'}$	ring def (B)
18b(SQ)	1117	1127	1132	$29H_{SQ1\phi} + 19K_{SQt} + 15H_{SQ\phi}$	C−H def (SQ)
18b(B)	1076	1088	1109	$41K_t + 40H_\phi$	C−H def (B)
18a(B)	1025	1033		$32H_\phi + 30K_t + 16H_\alpha$	C−H def (B)
1+12(B)	992	988		$39K_t + 24H_\alpha + 13K_{t'} + 13F^o_{(t,t)}$	ring def (B)
18a(SQ)	952	956		$39H_{SQ\alpha} + 31K_{SQt} + 20K_{SQ\phi}$	ring def (SQ)
6a(B)	830	825		$30H_\alpha + 21K_{t'} + 17K_{SQR'}$	X-sensitive (B)
N−H	785	759		$32H_{SQt} + 14H_{SQ\phi'} + 13H_{SQ\delta'}$	CNC def
6b(B)	630	618		$61H_\alpha + 15H_\phi$	ring def (B)

[a] / means not observable

to 1064 nm. Let us note that an uncertainty about the assignment of this band remains but it cannot be ascribed, as reported by some authors for the polymeric chain, to the C═N stretching mode because this kind of bond is not expected in this structure. By comparison with B2Q1, the softening of the C∼C bond adjacent to the amine group indicates the semiquinone-like character of this segment as we will see in the following. By a semiquinone-like character, we signify that the inner ring is the intermediate between an aromatic ring and a quinoid one. The increase of the 8a and 8b separation upon oxidation (26, 95, and 171 cm^{-1} for B3, $B3^{\circ+}$, and B2Q1, respectively) is consistent with this character.

In this spectral range, the vibrational modes 19a and 19b are also expected. These modes are due to a combination of C−H bending and CC stretching vibrations. By comparison with the IR features of B3 and B2Q1, the 19a and 19b modes of the external rings are ascribed to the absorptions whose maxima are at 1509 and 1453 cm^{-1}, respectively. The 19a and 19b modes of the inner ring are rather difficult to discern, and their assignment is the subject of numerous doubts. The IR absorption

at 1553 cm^{-1} is described as the vibrational mode 19b of the central ring. This absorption is observed between the similar modes for B3 (1450 cm^{-1}) and B2Q1 (1576 cm^{-1}) which introduces once again the semiquinone-like character of the central ring. The vibrational mode 19a is assigned to the absorption pointed at 1355 cm^{-1}. These modes are observed at 1558 (19b) and 1356 (19a) cm^{-1} in the IR spectrum of the polymeric chain.

The only Raman feature of the amine site ranged in this spectral domain occurs at 1501 cm^{-1}. This band is ascribed to the symmetric N−H deformation mode. Indeed, deuteration of the radical, performed by mixing B2Q1 with DCl, induces a shift of this peak to the low frequencies, at 1086 cm^{-1}. The IR antisymmetric N−H bending mode, which vibrates in a range particularly rich in bands, is rather difficult to discern. The absorption at 1537 cm^{-1} has been assigned to this amine mode.

(b) Region II: 1400−1000 cm^{-1}. In the 1400−1000 cm^{-1} spectral domain, the Raman spectra acquired with the wavelengths close to the maximum of the 387 and 700 nm absorptions differ from one another. They are characterized by two strong lines pointed at 1191 and 1375 cm^{-1} with the blue and red excitation lines, respectively.

This frequency range is of particular interest because it corresponds to the domain of the stretchings of the intermediate CN bond (noted C∼N) i.e., the CN bond intermediate between the single and double CN bonds. The peak at 1375 cm^{-1}, resonantly enhanced with the red line, arises without ambiguity from the intermediate C∼N bond near the central ring. Indeed, on deuteration of the N−H site, this most intense vibration of the amine group shifts upward by about 39 cm^{-1}. We can note also that this C∼N symmetric stretching mode is present midway of the single (1223 cm^{-1}) and double (1517 cm^{-1}) CN stretching modes of B3 and B2Q1, respectively. The frequency position of this mode is chain length dependent. It gives rise to a double band observed at ca. 1320 cm^{-1} in the case of ES.[32] The downshift of about 55 cm^{-1} when we pass from the three-ring oligomer to the polymeric form reveals a lengthening of the N≈central ring bond length upon the increase of the chain length, and this indicates a delocalization of the π-electrons along the polyconjugated system. The antisymmetric C∼N stretching mode is assigned to the absorption pointed at 1447 cm^{-1}.

This amine mode is also observed by Raman spectroscopy (676.4 nm) at 1442 cm^{-1}. The Raman-activity of this band traduces probably the fairly local character of the experimental results. It can also be correlated to the non planar geometry of our molecule. However, it is unexpected that this character is only observed from this mode. The Raman-activity can also be associated to the presence of another conformer in our powder. Recently, we have put in evidence by quantum chemical calculations the presence of two conformers in N,N′-diphenyl-1,4-benzoquinonediimine in the solid-state (B2Q1).[37,38] However, let us note that in the case of B2Q1, the majority conformer (96%) corresponds to the non planar trans (*E*) conformation and the presence of the non planar cis (*Z*) conformer is only discernible in the low-frequency region. Moreover, the other conformer of the doped dimer (in solution) is characterized by an intense band observed at 1401 cm^{-1}, which is absent from our Raman spectra. However, X-ray diffraction (XRD) experiments are actually in progress in order to verify the eventual presence of other conformers.

The most intense Raman band of the C−N bonds adjacent to the external rings, the symmetric C−N stretching mode, gives rise to the peak recorded around 1223 cm^{-1} at all the excitation wavelengths. This N-ring stretching vibration is slightly perturbed by the central ring-nature. It is peaked at approximately the same frequency for B3 (1223 cm^{-1}) and B2Q1 (1214 cm^{-1}). The doping process seems to predominantly affect the C∼N bonds near the central ring.

The ring modes that are particularly interesting in this spectral range are the 9a modes. These modes arise from the in-plane C−H deformation vibrations. Their interest lies in the fact that these vibrations are rather sensitive to the ring nature. For example, the 9a mode gives rise to a band observed around 1180 and 1160 cm^{-1} for the aromatic and quinoid paradisubstituted rings, respectively. For the doped dimer, the line at 1191 cm^{-1} is assigned to the 9a mode of the outer rings. The peak at 1191 cm^{-1} is only discernible in the spectrum performed at 457.9 nm, which suggests that the vibrational modes relative to the external rings are particularly enhanced with this wavelength. Let us remember that the 8a mode (1628 cm^{-1}) of the ending groups is the only intense band observed in the Raman spectrum in the 1700−1400 cm^{-1} range with the blue line. For the inner ring, the C−H bending mode is ascribed to the peak pointed at 1172 cm^{-1}. This mode is midway from its homologue for B3 (1182 cm^{-1}) and B2Q1 (1157 cm^{-1}), which suggests once again that the central ring of the model molecule of ES is intermediate between an aromatic ring and a quinoid one. The frequency position of the 9a mode is rather insensitive to the increase of the chain length. This mode gives rise to the bands centered at 1192 and 1166 cm^{-1} in the spectra of the polymeric chain with the blue and red lines, respectively.

Except the bands at 1375 and 1191 cm^{-1}, the 1400−1000 cm^{-1} spectral range is characterized by other bands of low intensity. The weak signals at 1001, 1027, and 1154 cm^{-1} correspond to the vibrational modes 1+12, 18a, and 15, respectively. These modes characteristic of the outer rings are enhanced with the blue line. As predicted by group theory, they are infrared-active. The weak IR line at 1076 cm^{-1} corresponds to the 18b mode of the outer rings. These bands, also recorded in the spectra of B3 and B2Q1, are considered to be fingerprints of the monosubstituted aromatic rings. These experimental results show that no noticeable frequency change takes place upon doping for the outer rings. These rings, enhanced with the blue line, keep their aromatic-like character. The modifications induced by doping can be considered as being mainly localized on the inner ring and its adjacent amine groups.

(c) Region III: 1000−600 cm^{-1}. In the low-frequency region (<1000 cm^{-1}), the assignment is rather delicate because the in-plane and the out-of plane modes are observed simultaneously. Nevertheless, by comparison with the vibrational features of B3 and B2Q1, some differentiation of the normal modes relative to the inner ring from those relative to the outer rings, slightly perturbed by the substituent nature, is made easier. Thus, the Raman bands at 602 and 828 cm^{-1} are assigned to the 6b and 6a normal modes of the outer rings, respectively. These two peaks are due to the CCC bending vibration. The IR absorptions at 690 and 743 cm^{-1} are ascribed to the vibrations 4 and 11. Vibration 4 is ascribed to the out-of-plane C−C stretching mode, and the mode 11 corresponds to the out-of-plane C−H deformation of the five adjacent phenyl hydrogens. These two absorptions are very useful because they provide information about the substitution pattern and inform consequently about the aromatic and monosubstituted character of the outer rings.

For the inner ring, the characteristic bands are observed at 801 and 614 cm^{-1} by Raman Scattering and at 845 cm^{-1} by IR absorption. The peak at 801 cm^{-1}, enhanced with the red line,

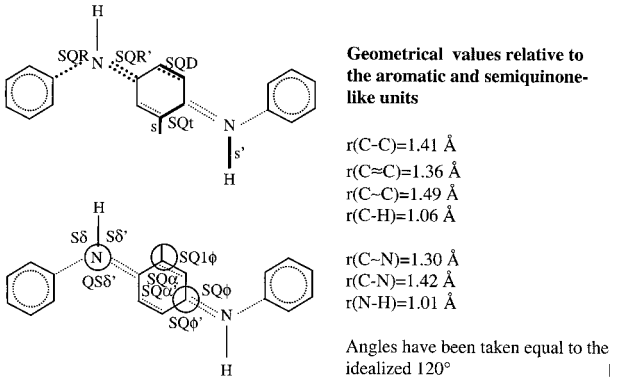

Figure 9. Definition of the internal coordinates and geometrical values.

corresponds to the ring breathing mode. This vibration is observed at 810 cm^{-1} in the Raman spectra of ES. The weak line at 614 cm^{-1} is ascribed to the ring deformation 6b. The absorption at 845 cm^{-1} is assigned to the mode 11. This out-of-plane mode is peaked at 814 and 856 cm^{-1} in the spectra of B3 and B2Q1, respectively, which indicates once again the semiquinone-like character of the inner ring.

The most intense feature of the N−H group is centered at 876 cm^{-1}. This peak, intense at 457.9 nm, is assigned to the N−H out-of-plane bending vibrational mode. This mode is also observed as a weak band at 676.4 nm and by IR spectroscopy.

4. Vibrational Calculations

A. **Methodology.** Our vibrational calculations are based on a valence force field model using the formalism of the Fourier dynamic matrix (For more details, see ref 31). Such analysis provides useful information about the structural and electronic changes upon radical formation, as manifested in the vibrational spectra, and more particularly in the force constants (interatomic forces) defined by eq 1

$$F_{\mathrm{SQR,SQR'}} = \left(\frac{\partial^2 \varphi}{\partial \mathrm{SQR}\ \partial \mathrm{SQR'}}\right)_0 \qquad (1)$$

.

To acquire the calculated frequencies (eigenvalues of the **F** matrix), the sets of force constants and the bidimensional representation (Potential Energy Distribution) of the vibrational normal modes, a set of internal coordinates (Figure 9) must be defined, and some parameters such as geometrical parameters (bond lengths and angles), atomic masses, and an initial set of force constants must be injected in the valence force field model.

A coherent set of force constants is expected when the experimental frequencies are less or as numerous than the fitted number of force constants. Thus, some practical considerations have been done in order to limit the calculations based on the observed frequencies of the doped dimer. Let us note that the vibrational fingerprints of the isolated molecule[32] (in solution) are analogous to these data suggesting that the crystal field effect is rather negligible.

i. The mutual exclusion principle being rather well verified in the 1700−600 cm^{-1} frequency range, the molecule was assumed centrosymmetric.

ii. The dimer was taken with a planar geometry allowing to distinguish between in-plane and out-of-plane vibrational modes.

iii. The starting set of force constants was stemmed from the vibrational analysis of B2Q1 concerning the carbon skeleton and of B3 for the amine group. The coupling constants relative to the quinoid unit which value is less than 0.1 mdyn $Å^{-1}$ (mdyn Å rad^{-2} and mdyn rad^{-1}) [31] have been transferred equal to zero in the semiquinone force constants set. The force constants of the external rings are taken similar to those of the aromatic unit with some exceptions (Table 3), the results acquired at 457.9 nm being close to those obtained in neutral B3.

iv. The C−H and N−H stretching modes are not included in the force field refinement because of the usual uncertainty in their assignments.

v. Bond length and angles have been taken similar to those of B2Q1 (Figure 9). Indeed, no geometrical parameters of the doped dimer have been reported until now.

vi. The refinement procedure was accomplished by continuously verifying the coherence of the force constants with regards to the others. The difference between each of the calculated frequencies ($\omega_{i\ \mathrm{calcd}}$) and the corresponding observed frequencies ($\omega_{i\ \mathrm{exp}}$) is refined by a least-squares fitting procedure where the standard deviation X given by eq 2 is minimized.

$$X = \left[\frac{1}{N}\sum_{i=1}^{N}\left(\omega i_{\mathrm{exp}} - \omega i_{\mathrm{calcd}}\right)^2\right]^{1/2} \qquad (2)$$

where N is the number of observed frequencies included in the refinement.

B. **Force Constants and Potential Energy Distribution (PED)**. Starting with the force fields of B2Q1 and B3, the calculated frequencies are in good agreement with the observed fundamentals (*X* ca. 8 cm^{-1}). The experimental and calculated data are listed in Tables 1 and 2 with tentative assignments. The PED expressed in terms of the force constants are also reported in these Tables. For more simplicity, the main force constants (diagonal force constants), and the calculated frequencies are discussed according to the ring nature. Moreover, to show by a most efficient way the evolution of the force constants, they are referencing to the force constants of the aromatic and quinoid segments. The definition of the force constants and their optimized value are summarized in Table 3.

(a) Normal Modes of the Aromatic-Like Character Ring. The calculated frequencies relative to the two external rings are in good agreement with the experiments. An inspection of the PED shows the vibrational mode 8a (70% C−C stretching), calculated at 1628 cm^{-1}, is in origin of the highest Raman frequency. The 8b mode (70% C−C stretching) is calculated at a frequency located between the 8a mode of the two segments present in the doped dimer, at 1612 cm^{-1}. The 19a and 19 IR modes, calculated at 1520 and 1462 cm^{-1}, are overestimated by the calculations, which is rather usual for these modes. They are a combination of CCH bending (60%) and C−C stretching (about 40%). The 9a mode, calculated at 1193 cm^{-1} and observed at 1191 cm^{-1}, possesses a predominant C−H bending character (65%).

The force constant H_ϕ contributing to the 9a mode was refined, and its value (0.52 mdyn Å rad^{-2}) is slightly larger than the H_ϕ force constant of the aromatic ring (0.50 mdyn Å rad^{-2}). The C−C stretching force constants have been taken as for them similar to those of the aromatic unit.

Considering that only three force constants were refined, the vibrations of the outer rings are rather well-reproduced by calculations. Thus, the bands observed at 1327 (3), 1270 (14), 1154 (15), 1076 (18b), 1027 (18a), 1001 (1 + 12), 828 (6a), and 602 (6b) cm^{-1} are calculated at 1359, 1252, 1158, 1088, 1033, 988, 832, and 607 cm^{-1}, respectively.

TABLE 3: Comparison of the Force Constants Relative to the Semiquinone-like Unit (and aromatic-like unit in parentheses) with Those Relative to the Fully Reduced and Oxidized Units

symbol	reduced unit	semiquinone-like unit	oxidized unit	symbol	reduced unit	semiquinone-like unit	oxidized unit
diagonal force constants: stretch (mdyn Å^{-1})				$F^m_{(SQt, SQt)}$	− 0.38	0	0
K_{SQD}	6.21	7.80	8.24	$F^o_{(SQt, SQt)}$	0.80	0.29	0.21
K_{SQt}	6.32	4.80	4.51	$F_{(SQR', s')}$	−0.31	− 0.27	/
K_{SQR}	5.32	4.90	5.24	$F_{(SQR, s')}$	− 0.31	− 0.29	/
$K_{SQR'}$	5.32	7.48	9.10	*force constants of interaction: bend − bend* (mdyn Å rad^{-2})			
K_s	5.09	5.09	5.09	$F_{(SQ1\phi, SQ1\phi)}$	0.02	0	0.07
$K_{s'}$	6.21	6.21	/[b]	$F_{(SQ\phi', SQ\phi)}$	0.02	0	− 0.11
diagonal force constants: bend (mdyn Å rad^{-2})				$F_{(SQ\alpha, SQ\alpha)}$	0	0	0.03
$H_{SQ\phi}$	0.50	0.45 (0.52)[a]	0.29	$F_{(SQ\alpha, SQ\alpha')}$	0.15	0.10	− 0.07
$H_{SQ1\phi}$	0.50	0.53 (0.52)	0.62	$F_{(\phi', SQ\delta')}$	0.12	0.17	0.19
$H_{SQ\phi'}$	0.86	0.89	0.89	$F_{(SQ\phi', SQ\delta')}$	0.12	0.06	− 0.01
$H_{SQ\alpha}$	1.04	1.10	1.06	*force constants of interaction: stretch − bend* (mdyn rad^{-1})			
$H_{SQ\alpha'}$	1.17	0.79	0.64	$F_{(SQt, SQ\alpha)}$	0.11	0.18	0.12
$H_{SQ\delta'}$	1.21	1.32	1.78	$F_{(SQt, SQ\alpha')}$	0.36	0.41	0.49
$H_{S\delta'}$	0.68	0.72	/	$F_{(SQt, SQ\phi)}$	0.16	0.18	0.26
$H_{S\delta}$	0.68	0.62	/	$F_{(SQt, SQ\phi')}$	0.30	0.30 (0.40)	0.20
force constants of interaction: stretch − stretch (mdyn Å^{-1})				$F_{(SQR,\alpha')}$	−0.13	−0.09	−0.08
$F_{(SQR, t')}$	0.46	0.45	0.62	$F_{(SQR, SQ\delta')}$	0.44	0.44	0.61
$F_{(SQR, SQR')}$	0.72	0.60	0.54	$F_{(SQD, SQ1\phi)}$	0.16	0.16	0.08
$F_{(SQt, SQR')}$	0.46	0.50	0.53	$F_{(SQD, SQ\alpha)}$	0.11	0.31	0.54
$F_{(s, SQt)}$	0	0	0.05	$F_{(SQR', SQ\delta')}$	0.44	0.63	0.53
$F_{(s, SQD)}$	0	0	− 0.06	$F_{(SQR', SQ\alpha')}$	− 0.13	− 0.54	− 0.97
$F^p_{(SQD, SQD)}$	0.33	0	0.05	$F_{(s, SQ\phi)}$	/	0	0.01
$F^o_{(SQD, SQt)}$	0.80	0.39	0.35	$F_{(s, SQ1\phi)}$	/	0	0.08
$F^p_{(SQt, SQt)}$	0.33	0	/	$F_{(SQR, S\delta)}$	0.36	0.32	/
$F^m_{(SQD, SQt)}$	− 0.38	0	− 0.06	$F_{(SQR', S\delta')}$	0.36	0.45	/

[a] The force constants of the aromatic-like unit, which differ from those of the aromatic unit, are presented in parentheses. [b] Not present.

(b) Normal Modes of the Semiquinone-Like Character Ring. The vibrational modes corresponding to the inner ring are well reproduced by the calculations in particular in the 1700−1400 cm^{-1} range. The 8a mode, dominated by a strong stretching motion of the C≈C bonds nonadjacent to the amine group (69%), with a small contribution from the stretching of the C∼C bonds near the N−H site (15%), can be considered as a pure ring mode (calculated value at 1584 cm^{-1}). The 8b mode, calculated at 1478 cm^{-1}, contains a large contribution from C∼C stretching (19%) but also from CCH deformation (36%) because it mixes with the 19b vibration of the outer rings expected in its vicinity.

The 19a mode possesses a strong contribution from CCH deformation (ca. 25%) and C∼N stretching (ca. 30%). It contributes in the two modes calculated at 1450 and 1343 cm^{-1}. The two lines observed at 1447 (1442 cm^{-1} in Raman spectroscopy) and 1355 cm^{-1} are mixed modes (19a(SQ) + C∼N stretching), consequently. This mixed character is also discernible in the Raman spectra (symmetry differs) of aniline radical cation.[39] Due to the largest contribution in $H_{SQ1\phi}$ for the band at low frequency, the band observed at 1355 cm^{-1} has been ascribed to the 19a mode of the semiquinone-like unit. The 19b mode, ascribed to the band observed at 1553 cm^{-1}, is calculated at 1563 cm^{-1}. In this mode, the C≈C stretching force constant K_{SQD} (78%), and the CCH bending force constant $H_{SQ\phi}$ (13%) contribute.

The frequency of the 9a mode is well reproduced by dynamical calculations. This mode calculated at 1170 cm^{-1} is primarily a CCH bending motion (70%) with a partial contribution from the C≈C stretching motion (10%). The CCH bending character is found also in the vibrations at 1127 cm^{-1}, which is consistent with the value observed at 1117 cm^{-1} (mode 18b). The mode 18a calculated at 956 cm^{-1} and observed at 952 cm^{-1} is a combination of the CCC bending (40%) and C∼C stretching (30%) modes. The breathing mode of the inner ring observed at 801 cm^{-1} is correctly calculated at 805 cm^{-1}. A comparison of the diagonal force constants relative to the central ring with those of B3 and B2Q1 (Table 3) shows that the changes going on from the neutral state to the charged state occur in the direction from aromatic toward semiquinone-like character. In particular, the disparity between the force constants of the carbon−carbon bonds reflects the semiquinone-like character. Indeed, the C≈C bonds harden, whereas the C∼C bonds near the amine group lengthen (by comparison with B3). Moreover, whereas in B2Q1, the ratio $F_{(double)}/F_{(single)}$, representing double and single bonds, is about 2. This ratio becomes ca. 1.5 in the case of the doped dimer (and 1 for B3).

(c) Normal modes of the amine group. The stretching and bending vibrations involving the CN and N−H groups are correctly calculated.

The N−H bending mode, observed at 1501 cm^{-1}, is calculated at 1503 cm^{-1}. This mode is characterized by a strong CNH deformation character (60%). The two force constants contributing in this deformation mode ($K_{S\delta}$ = 0.62 mdyn Å rad^{-2} and $K_{S\delta'}$ = 0.72 mdyn Å rad^{-2}) are midway from their analogous for B3 (K_{δ} = 0.68 mdyn Å rad^{-2}). The IR corresponding mode, the antisymmetric N−H deformation, is calculated at 1499 cm^{-1}. Several bands are discernible around this frequency in the IR spectrum and therefore, the assignment is not straightforward.

The most intense line of the CNC site, the symmetric C∼N stretching mode (adjacent to the inner ring) is observed and calculated at 1375 cm^{-1}. This normal mode is relatively pure (60% C∼N stretching character). The mode that also contains a large contribution of CN stretch is the antisymmetric stretching mode calculated at 1450 and 1343 cm^{-1}. The contribution from the C∼N stretching is more important for the band calculated at 1450 cm^{-1}, which is in agreement with our previous assignment. The force constant relative to the C∼N stretch ($K_{SQR'}$ = 7.48 mdyn Å^{-1}) is intermediate between its homologous for the C═N stretch ($K_{QR'}$ = 9.10 mdyn Å^{-1}) and the C−N stretch (K_R = 5.32 mdyn Å^{-1}) which consequently introduces the tendency of the CN bond length to decrease upon doping. These results are in agreement with XRD experiments[40] and

MNDO calculations[41] performed on the five-ring oligomer of ES. As an information, the CN stretching mode of aniline (ca. 1280 cm^{-1}) shifts up at ca. 1360 cm^{-1} upon removal of electron.[39]

The stretching mode of the C−N bonds adjacent to the outer rings observed at 1223 cm^{-1} is well reproduced by calculations (calculated value at 1225 cm^{-1}). The force constant involving in this mode is less than its homologous for B3, which indicates a softening of this bond with respect to the reduced dimer.

5. Conclusion

In this paper, we have proposed for the first time a detailed assignment of the in-plane fundamental normal modes, ranged from 1700 to 600 cm^{-1}, of a three-ring model molecule of ES. Using a valence force field model, two sets of force constants leading to a rather good agreement between the observed and calculated frequencies of the doped dimer have been obtained.

The experimental results conjugated with force field calculations indicate that the aromatic inner ring of B3 changes to a semiquinone-like ring upon removal of an electron. In particular, the 8a and 8b separation is consistent with this semiquinone-like character, and the analysis of the changes in the force constants (Carbon−Carbon stretching modes) permits us to clearly put the ring nature in evidence. The semiquinone-like character of the inner ring(s) of the five-ring oligomer of ES has also been emphasized by quantum-chemical calculations[41] and XRD experiments.[40]

The vibrational analysis shows also that the outer rings keep their aromatic-like character upon doping. Indeed, the Raman characteristics of the doped dimer recorded at 457.9 nm, wavelength which is known to clearly enhance reduced segments, is quasi superimposable to the one of the reduced dimer. Consequently, the force constants relative to this unit are taken in majority similar to those of the reduced segment and the calculated frequencies relative to the ending monosubstituted rings are analogous to the observed values.

Raman and IR spectroscopies reveal that when the chain length is short (three rings), geometrical changes going on from the neutral state to the cation, occur mainly close to the central ring and particularly to its adjacent C∼N bonds. The frequency of the modes relative to the amine group increases strongly (by ca. 180 cm^{-1} for the C∼N stretching mode), and the frequency of those relative to the inner ring shift slightly toward the low frequencies. These changes become more important in the infinite chain case (doublet at ca. 1320 cm^{-1}). These results can be correlated to X-ray Photoelectron Spectroscopy (XPS) and electron paramagnetic resonance (EPR) measurements performed on ES and its oligomers.[42] Indeed, XPS data show that the bands characteristic of the −NH− and =N− sites are clearly shifted upon doping, whereas those relative to the carbon atoms are not or slightly affected (no measurable chemical shift).[43] Moreover, EPR investigations of the dimer and other oligoanilines[44] have shown that the net charge is distributed on the amine group.

With the exception of the band ascribed to the symmetric C∼N stretching mode, the Raman spectra of the three-ring oligomer are very similar to those of the corresponding polymeric chain. The polymer can be considered to consist in the aromatic and semiquinone-like units, consequently. It is probable that the C∼N stretching mode can be considered as the key band that informs us about the delocalization of the charge.

Regarding the large literature devoted to conducting polymers, we can note that the vibrational analysis of some conjugated polymers combined with a model compounds approach permitted to put in evidence the nature of the major species (polarons and/or bipolarons) generated by the doping in the polymeric chain. The ratio of these different charged species for some polymers depends on the extent of the doping.[45] In the case of polyaniline family, a selective enhancement of the vibrational modes of the aromatic or semiquinone-like units is achieved upon selected excitation in resonance with the different chromophores. By studying this short oligomer, we cannot differentiate the vibrational features of the polaronic lattice from those of the bipolaronic form, consequently. Probably, a similar study performed on longest oligoanilines would permit the detection of the charge carriers' nature. This kind of investigation would also allow us to check the transferability of our sets of force constants and our proposal of assignment to state if polarons and bipolarons coexist in the only conducting form of polyaniline and, finally, to obtain information on the extent of conjugation and delocalization length. As pointed out recently by A. G. MacDiarmid et al.,[46] relatively few papers concerning oligoanilines are reported in the literature until now, whereas an enormous body of knowledge was accumulated for other oligomers, such as oligothiophenes[47,48] and oligo(phenylenevinylene)s.[49] This lack of interest is due in particular to the fact that these molecules are difficult to prepare. However, it seems that this tendency is being reversed, as some papers have recently been devoted to their preparation[50−52] and sensors using octaaniline and tetraaniline have been realized.[53]

References and Notes

(1) Kang, E. T.; Neoh, K. G.; Tan, K. L. *Prog. Polym. Sci.* **1998**, *23*, 277.
(2) Quillard, S.; Louarn, G.; Lefrant, S.; MacDiarmid, A. G. *Phys. Rev. B* **1994**, *50*, 12 496.
(3) MacDiarmid, A. G.; Epstein, A. J. *Faraday Discuss. Chem. Soc.* **1989**, *88*, 317.
(4) Chiang, J. C.; MacDiarmid, A. G. *Synth. Met.* **1986**, *13*, 193.
(5) See, for example: Proceedings of the International Conference of Science and Technology of Synthetic Metal; Montpellier, 1998 [*Synth. Met.* **1999**, *101−103*].
(6) Amano, K.; Ishikawa, H.; Kobayashi, A.; Satoh, M.; Hasegawa, E. *Synth. Met.* **1994**, *62*, 229.
(7) Barbero, C.; Miras, M. C.; Schnyder, B.; Haas, O.; Kötz, R. *J. Mater. Chem.* **1994**, *4*, 1775.
(8) Bernard, M.-C.; Hugot-Le Goff, A.; Zeng, W. *Electrochim. Acta* **1999**, *44*, 781.
(9) Cui, G.; Lee, J. S.; Kim, S. J.; Nam, H.; Cha, G. S.; Kim, H. D. *Analyst* **1998**, *123*, 1855.
(10) Syu, M.-J.; Liu, J. Y. *Sensors Actuators B* **1998**, *49*, 186.
(11) Syu, M.-J.; Liu, J. Y. *Sensors Actuators B* **1998**, *50*, 1.
(12) Karyakin, A. A.; Lukachova, L. V.; Karyakina, E. E.; Orlov, A. V.; Karpachova, G. P. *Anal. Commun.* **1999**, *36*, 153.
(13) Weissling, B.; Posdorfer, J. *Electrochim. Acta* **1999**, *44*, 2139.
(14) Brusic, V.; Angelopoulos, M.; Graham, T. *J. Electrochem. Soc.* **1997**, *144*, 436.
(15) Saprigin, A. V.; Brenneman, K. R.; Lee, W. P.; Long, S. M.; Kohlman, R. S.; Epstein, A. J. *Synth. Met.* **1999**, *100*, 55.
(16) Keuren, E. V.; Möhwald, H.; Rozouvan, S.; Schrof, W.; Belov, V.; Matsuda, H.; Yamada, S. *J. Chem. Phys.* **1999**, *110*, 3584.
(17) Martin, R. E.; Diederich, F. *Angew. Chem., Int. Ed.* **1999**, *38*, 1350.
(18) Riul, A., Jr.; Dhanabalan, A.; Mattoso, L. H. C.; de Souza, L. M.; Ticianelli, E. A.; Oliveria, O. N., Jr. *Thin Solid Films* **1998**, *327−329*, 57.
(19) Heinze, J.; Tschuncky, P.; Smie, A. *J. Solid State Electrochem.* **1998**, *2*, 102.
(20) Painelli, A.; Del Freo, L.; Girlando, A.; Soos, Z. G. *Phys. Rev. B* **1999**, *60*, 8129.
(21) Sakamoto, A.; Furukawa, Y.; Tasumi, M. *J. Phys. Chem. B* **1997**, *101*, 1726.
(22) Louarn, G.; Buisson, J. P.; Lefrant, S.; Fichou, D. *J. Phys. Chem.* **1995**, *99*, 11 399.
(23) Orion, I.; Buisson, J. P.; Lefrant, S. *Phys. Rev. B* **1998**, *57*, 7050.
(24) Hernandez, V.; Castiglioni, C.; del Zoppo, M.; Zerbi, G. *Phys. Rev. B* **1994**, *50*, 9815.
(25) Furukawa, Y. *J. Phys. Chem.* **1996**, *100*, 15644.

(26) Heeger, A. J.; Kivelson, S.; Schrieffer, J. R.; Su, W. P. *Rev. Mod. Phys.* **1998**, *60*, 781.
(27) Brédas, J. L.; Chance, R. R.; Silbey, R. *Phys. Rev. B* **1982**, *26*, 5843.
(28) Chance, R. R.; Brédas, J. L.; Silbey, R. *Phys. Rev. B* **1984**, *29*, 4491.
(29) Xie, S. J.; Mei, L. M. *J. Phys.: Condens. Matter* **1994**, *6*, 3909.
(30) Zaghal, M. H.; Shatnawi, *M. Y. Org. Prep. Proced. Int. Briefs* **1989**, *21*, 364 *Chem. Abstr* 112, 234 879b.
(31) Boyer, M. I.; Quillard, S.; Rebourt, E.; Louarn, G.; Buisson, J. P.; Monkman, A.; Lefrant, S. *J. Phys. Chem. B* **1998**, *102*, 7382.
(32) Boyer, M. I.; Quillard, S.; Cochet, M.; Louarn, G.; Lefrant, S. *Electrochim. Acta* **1999**, *44*, 1981.
(33) Louarn, G.; Lapkowski, M.; Quillard, S.; Pron, A.; Buisson, J. P.; Lefrant, S. *J. Phys. Chem.* **1996**, *100*, 6998.
(34) Ping, Z.; Nauer, G. E.; Neugebauer, H.; Theiner, J.; Neckel, A. *J. Chem. Soc., Faraday Trans.* **1997**, *93*, 121.
(35) Wilson, E. B. *Phys. Rev.* **1934**, *45*, 706.
(36) Furukawa, Y.; Hara, T.; Hyodo, Y.; Harada, I. *Synth. Met.* **1986**, *16*, 189.
(37) Choi, C. H.; Kertesz, M.; Boyer, M. I.; Cochet, M.; Quillard, S.; Louarn, G.; Lefrant, S. *Chem. Mater.* **1999**, *11*, 855.
(38) Boyer, M. I.; Choi, C. H.; Kertesz, M.; Cochet, M.; Quillard, S.; Lefrant, S.; Louarn, G. *Synth. Met.* **1999**, *101*, 784.
(39) Brouwer, A. M.; Wilbrandt, R. *J. Phys. Chem.* **1996**, *100*, 9678.
(40) Shacklette, L. W.; Wolf, J. F.; Gould, S.; Baughman, R. H. *J. Chem. Phys.* **1988**, *88*, 3955.
(41) Libert, J.; Brédas, J. L.; Epstein, A. J. *Phys. Rev. B* **1995**, *51*, 5711.
(42) Rodrigue, D.; Domingue, M.; Riga, J.; Verbist, J. J. *Synth. Met.* **1993,** *55*−*57*, 4802.
(43) Neoh, K. G.; Kang, E. T.; Tan, K. L. *J. Phys. Chem. B* **1997**, *101*, 726.
(44) Wienk, M. M.; Janssen, R. A. J. *J. Am. Chem. Soc.* **1997**, *119*, 4492.
(45) Chakrabarti, S.; Das, B.; Banerji, P.; Banerjee, D.; Bhattacharya, R. *Phys. Rev. B* **1999**, *60*, 7691.
(46) MacDiarmid, A. G.; Zhou, Y.; Feng, J. *Synth. Met.* **1999**, *100*, 131.
(47) Nakanishi, H.; Sumi, N.; Aso, Y.; Otsubo, T. *J. Org. Chem.* **1998**, *63*, 8632.
(48) Hernandez, V.; Casado, J.; Kanemitsu, Y.; López Navarrete, J. T. *J. Chem. Phys.* **1999**, *110*, 6907.
(49) Stampfl, J.; Tash, S.; Leising, G.; Scherf, U. *Synth. Met.* **1995**, *71*, 2125.
(50) Sadighi, J. P.; Singer, R. A.; Buchwald, S. L. *J. Am. Chem. Soc.* **1998**, *120*, 4960.
(51) Wei, Y.; Yang, C.; Wei, G.; Feng, G. *Synth. Met.* **1997**, *84*, 289.
(52) Gao, J.; Li, K.; Zhang, W.; Wang, C.; Wu, Z.; Ji. Y.; Zhou, Y.; Shibata, M.; Yosomiya, R. *Macromol. Rapid Commun.* **1999**, *20*, 560.
(53) Feng; J.; MacDiarmid A. G. *Synth. Met.* **1999**, *102*, 1304.